

Article

Study on the Influence of Initial State on Loess Erosion Characteristics and Microscopic Mechanism

Hong Zheng^{1,2}, Xi-An Li^{1,*}, Ya-Hong Deng¹, Zhi-Tao Hao¹ and Feng Wen¹¹ College of Geological Engineering and Geomatics, Chang'an University, Xi'an 710054, China² China Electronic Research Institute of Engineering Investigations and Design, Xi'an 710001, China

* Correspondence: dclixa@chd.edu.cn

Abstract: Because of its loose, porous, and vertical structure, loess easily absorbs water, and it contains a large amount of soluble material, making it susceptible to erosion by water flow from rainfall or irrigation, with potentially disastrous consequences. Damage can result especially from loess slope erosion. In this paper, physical tests and microscopic analysis are used to study loess erosion. The purpose is to explore the internal structure of the soil caused by the infiltration of the water body when it flows through the loess slope, and thus to learn more about the internal mechanisms of surface erosion caused by the migration and relocation of the soil particles on the surface of the slope. Erosion tests of samples with different dry density and water content were carried out. It was found that the amount of erosion decreases with an increase of dry density and increases with an increase of water content. Through physical simulation tests combined with field investigation and analysis, the entire erosion process is divided into four erosion characteristic stages: uniform surface erosion; micro drop pit erosion; micro drop pit bead erosion; and rill erosion. The erosion mechanism and micro mechanism of different erosion characteristics are analyzed and summarized. The influences of different dry density and water content on the erosion process are analyzed and summarized, and the internal mechanism of erosion is revealed from the perspective of microstructure, thereby providing a sound basis for engineering construction and erosion-related disaster management in the Loess Plateau.



Citation: Zheng, H.; Li, X.-A.; Deng, Y.-H.; Hao, Z.-T.; Wen, F. Study on the Influence of Initial State on Loess Erosion Characteristics and Microscopic Mechanism. *Sustainability* **2023**, *15*, 4676. <https://doi.org/10.3390/su15054676>

Academic Editor: Mingming Guo

Received: 13 February 2023

Revised: 2 March 2023

Accepted: 3 March 2023

Published: 6 March 2023



Copyright: © 2023 by the authors. Licensee MDPI, Basel, Switzerland. This article is an open access article distributed under the terms and conditions of the Creative Commons Attribution (CC BY) license (<https://creativecommons.org/licenses/by/4.0/>).

Keywords: loess slope; water erosion; erosion characteristics; microstructure

1. Introduction

Loess is a kind of yellow or yellowish-brown soil-like sediment composed mainly of silt. It is rich in carbonates, has large pores, and is widely distributed in the world. The Loess Plateau of China is the largest continuous body of loess in the world, with a total area of about 6.4×10^5 km², accounting for 6.3% of China's land area [1,2]. Slope erosion in the loess area of China is serious. Damage to loess slopes can include collapse, landslides, mudslides, and ground fissures, all of which, while disturbing the loess, also leave traces of undisturbed loess. It is a challenge to researchers to solve the problem of slope erosion in a way that minimizes the proportion of disturbed loess [3–5]. Understanding the microscopic mechanisms in soil erosion by water of loess slopes can help to prevent soil erosion.

In 1966, Pusch proposed the concept of flocs (aggregate structures) for observed clay slice images. These images are characterized by the connection of small particle groups between flocs or aggregates with higher density or between larger particles [6]. From 1967 to 1969, Morgan and Smart observed that clay tends to form aggregate structures when consolidated at high pressure [7,8]. With the gradual maturing of the theoretical basis and qualitative characterization of soil microstructure, research on soil microstructure gradually changed after the 1950s from broad theoretical research to quantitative research. In 1964, Brewer analyzed the structure and mineral content of soil in detail, providing a useful summary for an accurate quantitative description of the complex structure of

soil [9]. In 1966, Smart combined a spectrometer with a polarizing microscope to study the anisotropy of soil samples [10]. In 1975, Krizek et al. used scanning electron microscopy, optical microscopy, and X-ray diffraction to identify and quantify the structure of clay, and obtained a comprehensive evaluation of particle binding and orientation [11]. In 1980, Gao et al. studied the northern loess in China and classified it according to its particle morphology and arrangement [12]. Since then, significant research achievements have been made in understanding pore compression, particle arrangement, orientation, anisotropy, and the characteristics of connections between particles. Since the 1980s, the study of soil microstructure has been gradually combined with engineering practice. Many researchers have begun to study the changes of soil microstructure for different mechanical or working conditions. From 1984 to 1987, Lei et al. studied the pore structure of loess in the Xi'an area by mercury intrusion tests. Through the distribution characteristics of pores, these researchers inferred that porosity is the main cause of loess collapsibility. This insight provides a reliable basis for continued work on related geological problems such as loess collapsibility on the Loess Plateau [13–15]. Bazant and Pra, as well as Bazant and Bishop, have established micromechanical models for rock and concrete fracture [16,17]. In 1990, Li et al. conducted a quantitative study of the pores of cohesive soil, revealing the macro-micro contrast relationships among microstructure, pore size, and water conductivity [18,19]. In 1997, Munkholm used an X-ray computed tomography scanner to quantify the pore characteristics of undisturbed soil, and then linked these results to soil fragility assessed using the drop-breaking method [20]. Ni et al. studied the microstructure changes of loess from the perspectives of the freeze-thaw cycle, consolidation pressure, and soaking-wetting cycles, and explored the relationship between soil mechanical characteristics and microstructure [21–23]. These microstructure studies, based on different working conditions and common geological phenomena, have greatly promoted the connection between microstructure research and macroscopic soil properties. Thus, the study of loess microstructure has been carried out for nearly a century, going from qualitative to quantitative research. However, due to the complexity of test methods, there is still a lack of comprehensive research on the microscopic mechanism of soil erosion by water of loess slopes and the internal factors controlling erosion.

In this study, indoor physical simulation experiments combined with scanning electron microscopy experiments were used. Image-Pro Plus image processing software was used to process the microscopic images of loess samples under different initial conditions. The pore microstructure characteristics and variation rules of loess samples under different initial conditions were quantitatively analyzed. The erosion characteristics of loess samples under different initial conditions were studied, and the mechanism and microscopic details of slope erosion were revealed. The quantitative study of erosion characteristics from a microscopic perspective provides an important theoretical basis.

2. Materials and Methods

2.1. Experimental Materials

The soil samples used in this experiment were taken from the Shaanxi region of the Loess Plateau in China; the sampling site is shown in Figure 1. The sample is Q₃ Malan loess; its basic physical properties are shown in Table 1.

The mineral composition of the experimental materials was analyzed by a Bruker ASX D8 X-ray diffractometer, and the results are shown in Table 2. Its mineral composition includes principally quartz (Qtz), plagioclase (Pl), calcite (Cal), dolomite (Dol), illite (Il), potassium feldspar (Or), chlorite (Chl), and kaolinite (Kl).

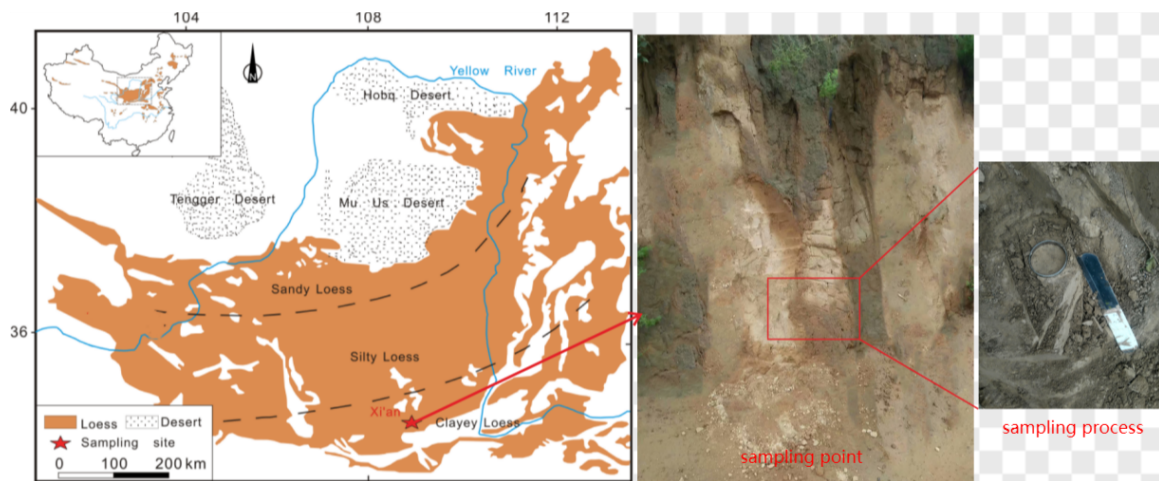


Figure 1. Location of the study site.

Table 1. Loess properties at the in-situ experimental site.

Dry-Density (g/cm ³)	Water Content (%)	Percent Clay $\Phi < 0.005$ mm	Percent Silt $\Phi < 0.074$ mm	Percent Sand $\Phi > 0.074$ mm	Hydraulic Conductivity (cm/s)
1.27	13.3	25.8	73.9	0.3	1.60×10^{-4}

Table 2. Loess chemical and mineral components at the in-situ experimental site.

Mineral Component (%)	Qtz	Pl	Cal	Or	Dol	Il	Chl	Kl
test result	40	17	11	2.4	1.6	21	4	3

2.2. Experimental Apparatus and Process

The test device was a self-developed loess sample scouring instrument (Figure 2), which is used mainly for indoor simulated scouring tests of large loess samples. This loess sample-scouring instrument is composed of three parts: water supply system, scouring system, and monitoring system. The water supply system uses a constant-flow tank. The scouring system includes mainly a scouring tank, energy dissipation tank, and sampler. The monitoring system consists of two high-speed cameras to monitor the erosion of the sample.

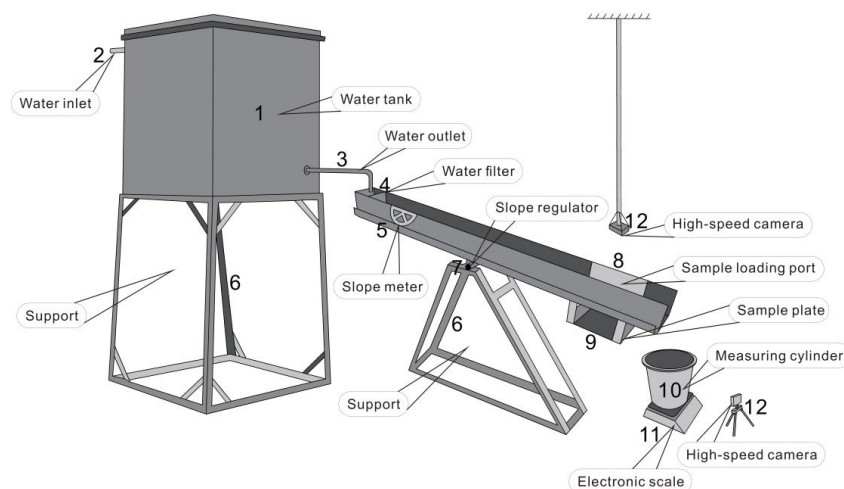


Figure 2. Apparatus used in the test.

The samples used in the instrument were rectangular samples measuring 10 cm × 20 cm × 10 cm (length × width × height). The initial dry densities of the samples were 1.2, 1.3, 1.4, 1.5, and 1.6 g·cm⁻³, and the initial moisture contents were 10%, 12%, 14%, 16%, and 18%, respectively. The sample preparation and test process are described and shown in Zheng et al. [24].

2.3. Microstructure Sample Preparation

The preparation of microscopic samples used the glue injection method. The specific process is as follows: (1) A cylinder with a height of 1.5 cm and a diameter of 1 cm was cut by a knife from the prepared loess samples for different initial conditions. (2) The sample was put into a soil sampler with a diameter of 1 cm. (3) A dropper was used to drop the cementation curing solution into the soil sampler until the consolidation solution submerged the sample—about 1 cm above its top surface. The purpose was to consolidate the soil sample, so that the consolidated solution filled the pores of the loess sample. (4) The sample was held at normal temperature and pressure. The cementation curing solution that was used is epoxy resin, acetone, ethylenediamine, and dibutyl phthalate. Its ingredients were combined in a ratio of 100:50:4:1, respectively. (5) After standing for a month, the sample was hardened, and the excess material around the sample was removed by a cutting machine. The sample was then put into a mold and poured into a special inlay material to completely solidify it and protect it from damage caused by subsequent grinding. (6) A special grinding instrument was used, so that the imaging surface was smooth and the image could be clearly identified. (7) The samples were placed on the scanning electron microscope stage for microscopic observation and image photography.

In this work, the pore classification standard proposed by Li et al. was used as a scale for classifying the pores. The pores were divided into large pores ($d > 32 \mu\text{m}$), medium pores ($8 \mu\text{m} < d < 32 \mu\text{m}$), small pores ($2 \mu\text{m} < d < 8 \mu\text{m}$), and micropores ($d < 2 \mu\text{m}$) [25]. The scanning electron microscope used in this study was an FEI Quanta 400 FEG, and IPP image processing software was used to process and analyze the microscope's photos.

3. Results and Discussion

3.1. Analysis of Scouring Process

A dry density of 1.2 g·cm⁻³, moisture content of 14%, and slope of spacing between 20 degree were selected to describe and explain the process and types of erosion on the loess slope, as shown in Figure 3. The specific scouring process can be divided into the following stages: (1) Uniform surface erosion stage. When water flowed down the slope, a small amount of loose soil scattered on the slope was taken away first. Because the slope was unsaturated loess, the soil seemed to be compacted, but the pores between the soil particles were filled with air. The water flowing down the slope infiltrated into the soil, gradually saturating the surface soil. The matrix suction between the particles was weakened, and the effect of buoyancy and permeability was added. The aggregate particles of the soil were disintegrated, and the soil particles were in the critical starting state. (2) A stage of micro-drop pit erosion. With an increase of water content, the cohesive force between soil particles gradually decreased. At this time, the infiltration of the whole soil was uneven. In the area with a high degree of infiltration, the surface water flow was greater than that in other areas. Due to the natural slight unevenness of the slope itself, the soil particles in the low-lying areas and areas with a high degree of infiltration were taken away by the water flow, leaving small pits. (3) An erosion stage of beaded micro-drop pits. As the water continued to scour, the number of small pits gradually increased. The water flow on the slope was unevenly distributed on the slope at this time, and the stability of the soil around the small drop pits was reduced. Therefore, when the water flowed through these small sinkholes, the energy was dissipated by the soil around the sinkholes, resulting in a further increase in the size of these sinkholes. As the erosion continued, the surface of the slope was randomly distributed with scaly surface erosion pits, and their number was gradually increasing. Some of them had a tendency to connect, and gradually extend to the top of

the slope, forming small grooves. (4) Rill erosion stage. With continued erosion of the water flow, multiple streams of runoff along the rill were formed on the slope. These runoff streams continued to influence the soil on and around the rill, resulting in continuous deepening of the rill. In the process of continuous expansion of the rill, runoff continued to be collected into the rill. At this time, at the bottom of the rill, if the soil with strong erosion resistance or the soil falling on both sides of the rill was blocked at the head of the rill, the runoff flowed from the blocking position to both sides, and there was bifurcation. Each rill was steadily widened, bifurcated, and merged due to uneven water flow erosion, and some rills eventually penetrated each other to form a slope rill grid, so that the gully head appeared to be eroded. At this time, the rill would gradually take on the appearance of a horn from the bottom to the top of the slope. The rill would continue to develop at the bottom of the slope, while the top of the slope would be eroded due to source erosion, and because it had first contact with the runoff, the erosion intensity was the largest there.

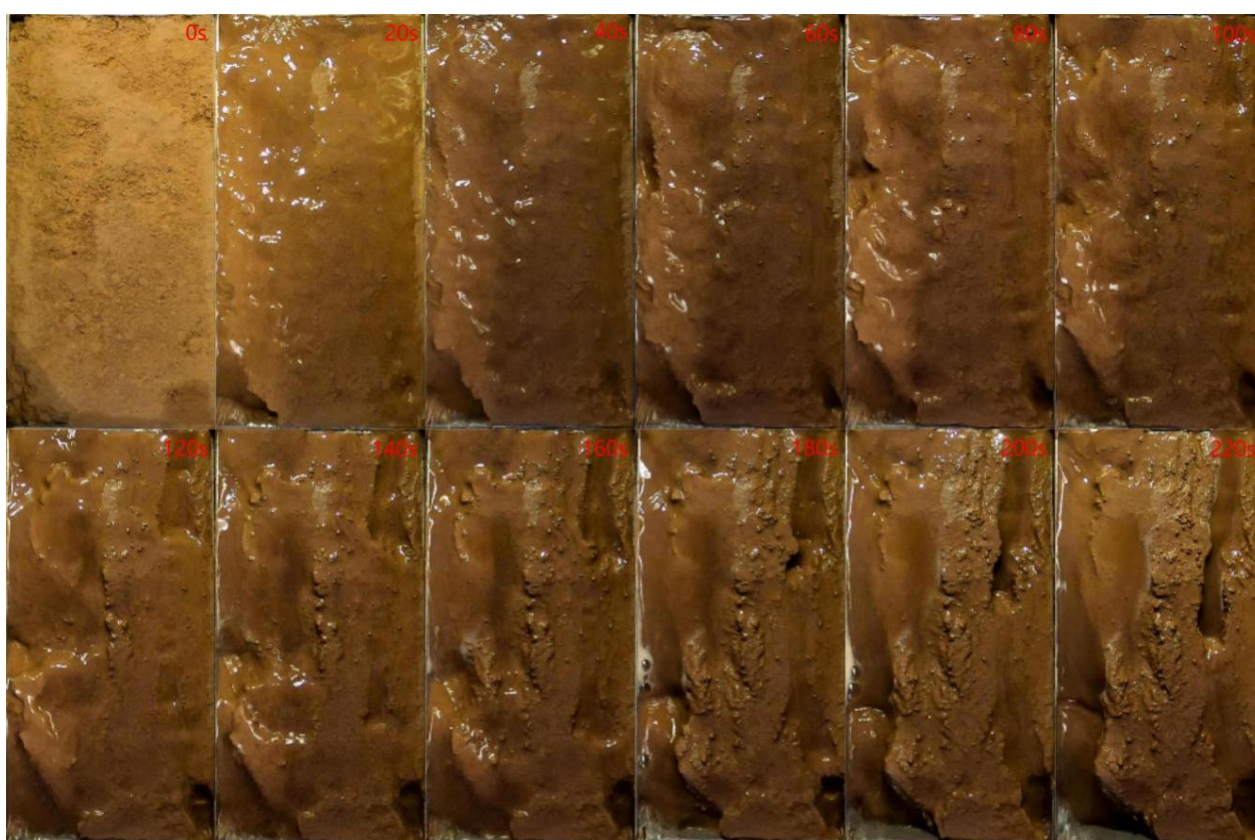


Figure 3. The erosion process of initial cross section of flow.

3.2. Influence of Initial Dry Density on Erosion Quantity

For the same initial water contents, amounts of erosion of loess samples for different initial dry densities are shown in Figure 4: (a) for 10%, (b) for 12%, (c) for 14%, (d) for 16%, (e) for 18%. It can be seen from this figure that the amount of erosion is inversely correlated with the initial dry density of the sample. When the initial water content of the loess was constant and the dry density increased, the original loose loess structure became denser, the contact area between the loess particles increased, the sliding friction force increased, the spacing between the loess particles decreased, the mutual attraction between the loess particles increased, and the attraction of the bound water to the surrounding loess particles increased. At the same time, after the loess particles were rearranged, the interlocking effect produced by their mutual connection was enhanced, and the friction and bonding forces between the particles that were needed to overcome damage became larger, the shear strength increased, and the amount of erosion became smaller.

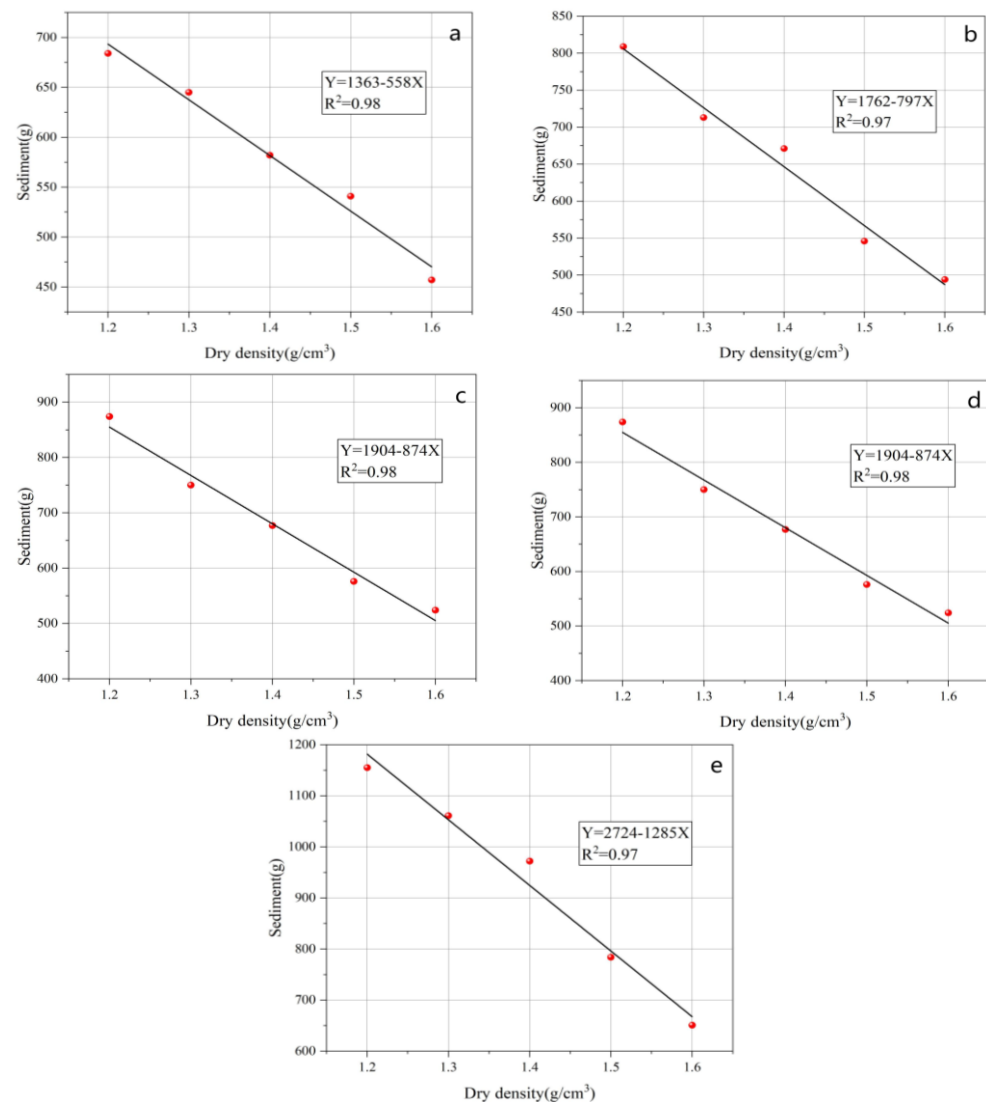


Figure 4. The relationship between loess sediment and the initial dry density.

3.3. Influence of Initial Water Content on Erosion Quantity

For the same initial dry density, the dependence of the amount of erosion of loess samples on initial water content is shown in Figure 5: (a) for $1.2 \text{ g}\cdot\text{cm}^{-3}$, (b) for $1.3 \text{ g}\cdot\text{cm}^{-3}$, (c) for $1.4 \text{ g}\cdot\text{cm}^{-3}$, (d) for $1.5 \text{ g}\cdot\text{cm}^{-3}$, (e) for $1.6 \text{ g}\cdot\text{cm}^{-3}$. It can be seen from this figure that the initial water content of the sample had a significant positive correlation with the amount of erosion—that is, for the same initial dry density, the amount of erosion of the loess sample increased with an increase of initial water content. In the case of a small water content, the loess particles were connected to each other by cementation to form a skeleton structure, so that the soil was structurally strong. As the water content of the soil sample increased, the strength of some cements between the particles of the loess skeleton were weakened by action of the water; the water film on the outer surface of the particles became thicker, the water film force became weaker, and the connection strength between the particles was weakened. The strongly bound water layer was finally converted into free water between the particles, the friction between the particles was reduced, the pore structure was destroyed, and the cement between the particles was dissolved, so that the structural strength of the soil was rapidly reduced, resulting in the compression deformation of the overhead structure inside the loess. The shear strength was reduced and the amount of erosion was increased.

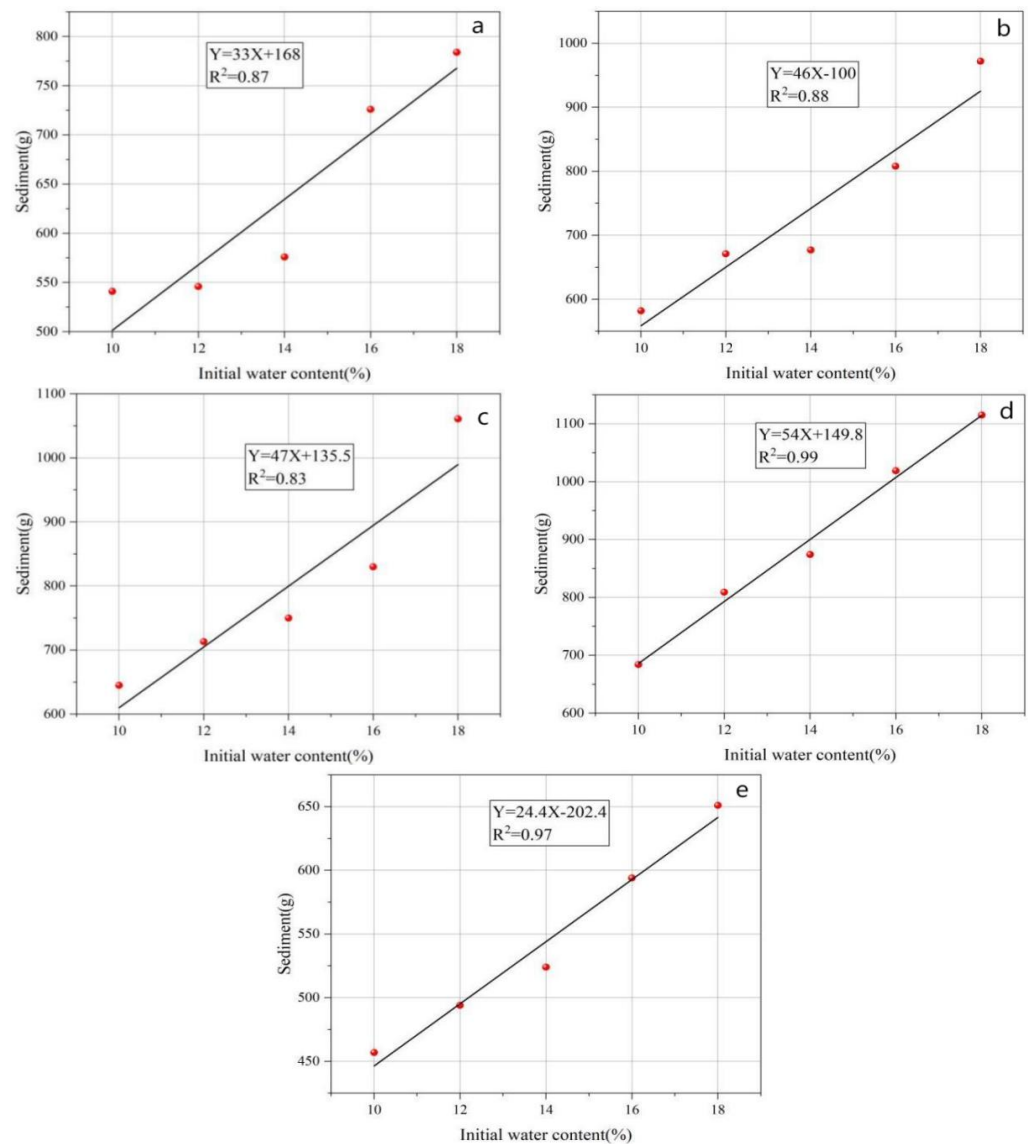


Figure 5. The inverse correlation between loess sediment and the initial water content.

4. Microscopic Mechanism Analysis

4.1. Microstructure of Loess Samples with Different Initial Dry Density

Figure 6 shows the electron microscope images of loess samples with an initial water content of 12% and dry density of 1.2, 1.3, 1.4, 1.5, and 1.6 $\text{g}\cdot\text{cm}^{-3}$. The pressure required for sample preparation of remolded loess increased with an increase of dry density. As the pressure increased, the particles were rearranged and were pressed closer together. The pores were also squeezed and deformed due to the rearrangement. The soil samples with small initial dry density had the most macropores, because the structure of loess samples with small dry density was looser than that of samples with large dry density, and the macropores were relatively more numerous. It can be seen from Figure 7: (a) for pore quantity, (b) for the average pore diameter, (c) pore area. And that the total number of pores increased. The numbers of mesopores, micropores, and small pores fluctuated as the dry density increased, but the overall trend was increasing, while the number of large pores decreased. The average diameter of micropores, small pores, and medium pores under different dry densities was basically stable, whereas, as the dry density increased, the average diameter of large pores decreased, and medium pores and small pores became dominant, indicating that the average size of pores decreased as the dry density increased. With an increase of dry density, small particles filled the pores, so there was a higher particle

content per unit volume and smaller pore area. As the dry density increased, the ratio of large-pore area to medium-pore area decreased gradually, and the area of micropores and small pores increased. This indicates that as the density increases, the decrease of total pore area of the soil sample begins with the large pores, then slowly transitions to the middle pores. Evidently, the dominance of soil pores gradually changed from large and medium pores to small and micropores. With a dry density of $1.2 \text{ g}\cdot\text{cm}^{-3}$, there were almost only large pores, small pores, and micropores in the soil sample, with few middle pores. This was because the dry density was small, the loess structure was loose, and the particles were aggregated. There were many forms, and the large pores existed between the aggregates that were gathered together, forming the overhead structure of the loess, whereas the micropores and small pores were mostly present inside the aggregates. With greater density of the loess structure, the pores between the aggregates mostly reached the size of the middle pores.

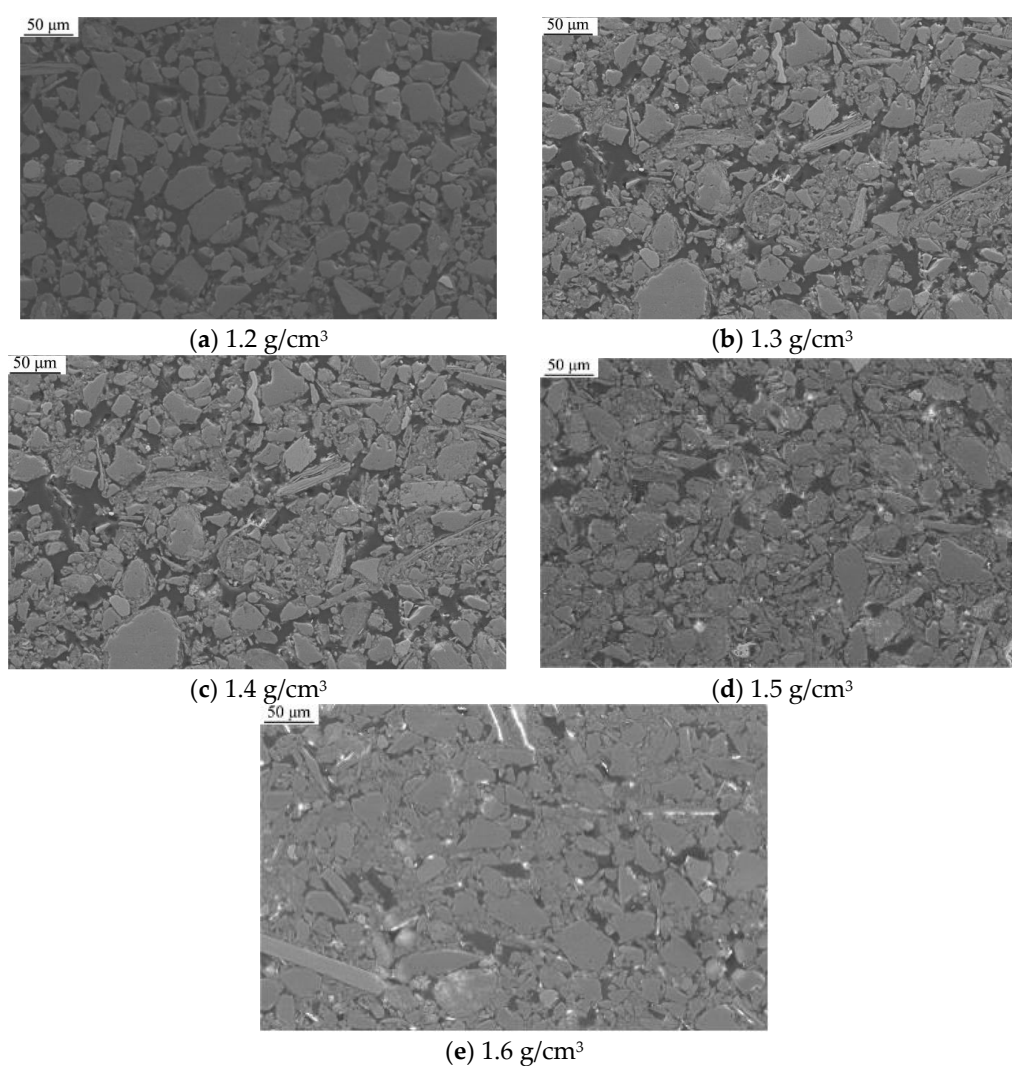


Figure 6. SEM images of loess samples with different dry densities.

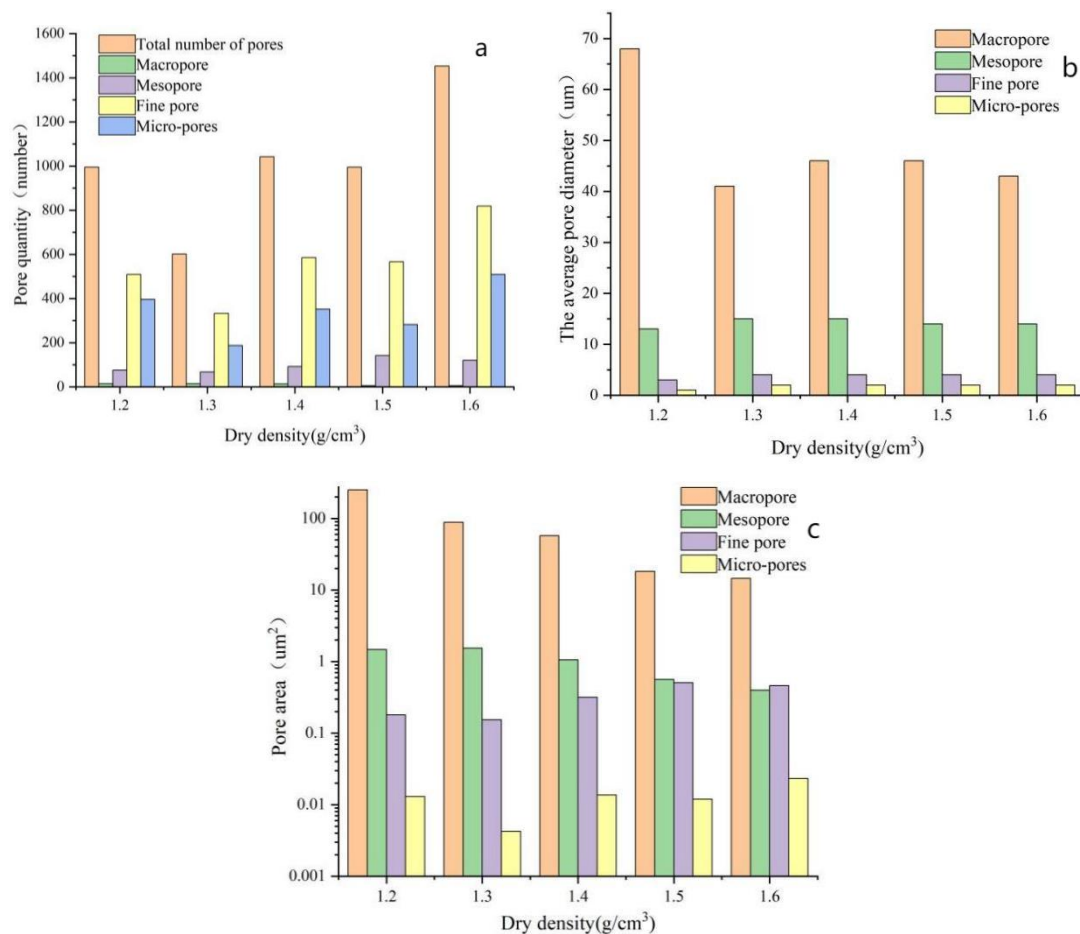


Figure 7. Micropore parameter curves of loess samples with different dry densities.

4.2. Microstructure of Loess Samples with Different Initial Water Content

Figure 8 shows scanning electron microscope images of loess samples with an initial dry density of $1.4 \text{ g}\cdot\text{cm}^{-3}$ and water content of 10%, 12%, 14%, 16%, and 18%. These SEM images of loess soil samples under different initial water content show that more aggregates appear in the soil samples prepared under relatively dry conditions (smaller initial water content). The microstructure of the loess is uneven and randomly arranged, depending on the irregularity and randomness of the clay body position. For low water content, the loess particles were mainly connected by surface cementation; the connection strength was large, and they were arranged in a mosaic. The skeleton particles were closely arranged and the pore space was small, resulting in a large matrix suction. The capillary action tended to connect the loess particles and clay together, and usually had a colloidal flocculation trend during sample preparation to form particle-clay aggregates. In this case, water was stored mainly in the aggregates, and the large pores between the single particles were occupied mainly by air. When the soil sample was prepared with a higher water content, the cementation connection between the particles was destroyed, and the particles experienced point contact-based connections, so that the structural strength decreased rapidly, and the close arrangement of the mosaic became an overhead loose arrangement. A large pore space led to a decrease of the matrix suction, instability of the micro-spatial structure system, and a decrease of the strength of the soil. The degree of flocculation between particles was reduced and the pore distribution is more uniform. The clay exhibits a more uniform distribution, and the clay particles are clearly visible between the skeleton's single particles and are connected together to fill the pores between the particles. In a state of high water content, water pushed the loess unit away during the sample preparation process, resulting in a dispersed structure. The difference between the microporous and

macroporous systems is no longer significant, and the pore distribution is more uniform. This is due to the dependence of the loess matrix on water content. When the initial water content was high, the capillary action decreased, the compressibility of the matrix increased, and it was easily affected by external force. Therefore, when the soil sample is compacted under high water content, not only will the pores between the aggregates change, but also the pores in some larger aggregates will change, making the pore distribution of the soil sample more nearly uniform. It can be seen in Figure 9: (a) for pore quantity, (b) for the average pore diameter, (c) pore area. And that as the water content increased, the number of micropores decreased. The number of small pores and mesopores increased first and then decreased, while the number of large pores increased significantly. The average diameter of micropores, small pores, and medium pores was basically stable, while the average diameter of large pores increased significantly. The pore area of macropores also showed a significant increasing trend, while the pore area of mesopores increased first and then decreased, and the pore area of micropores showed an increasing trend.

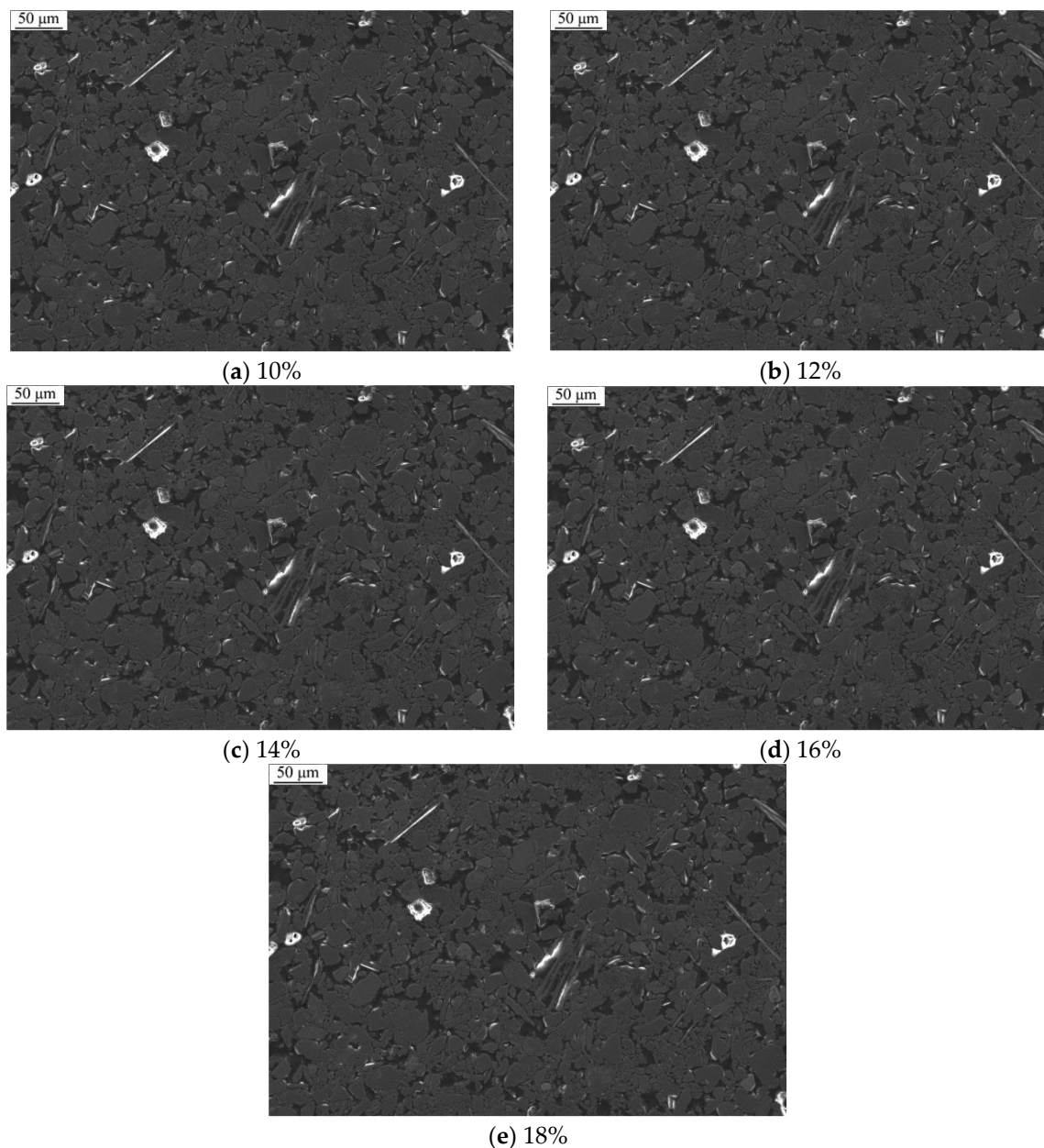


Figure 8. SEM images of loess samples with different moisture contents.

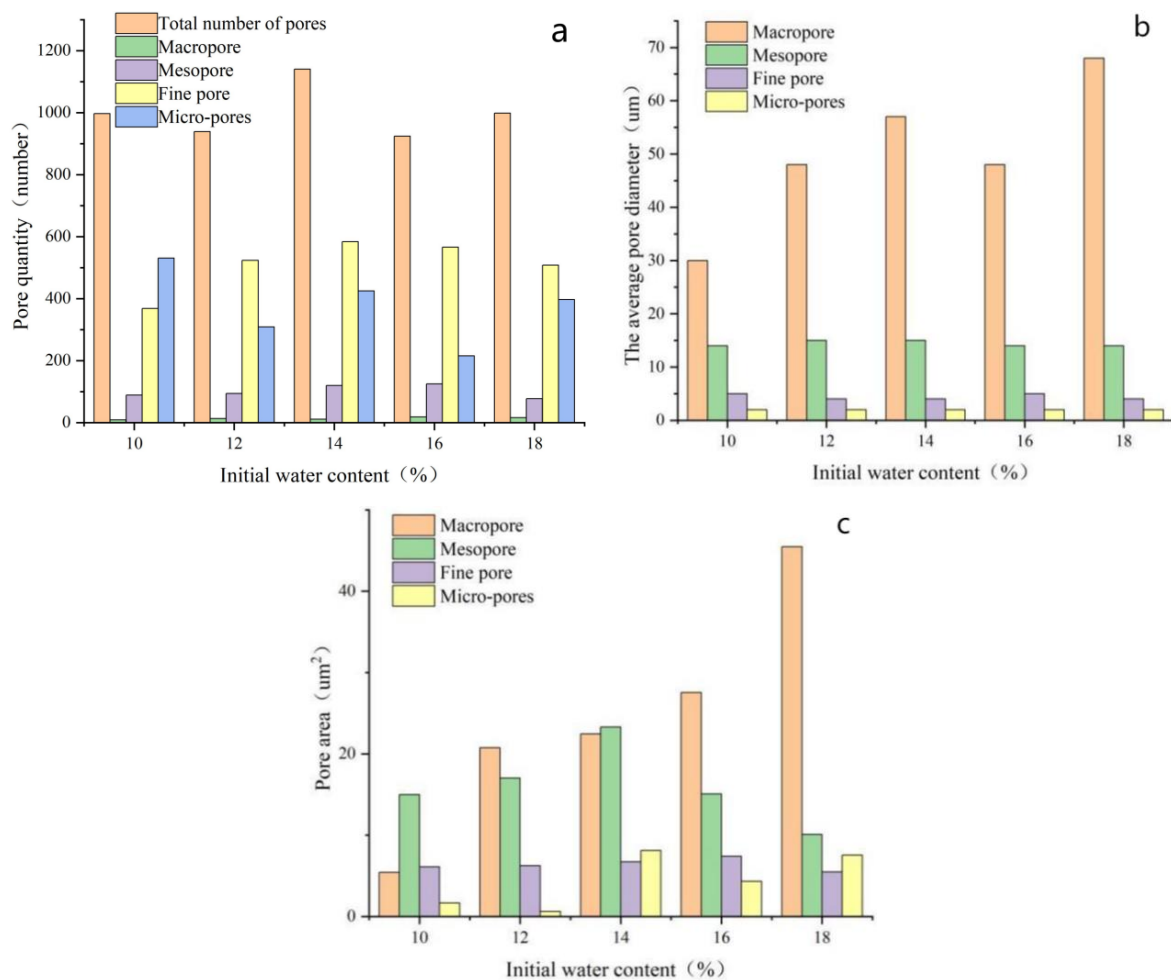


Figure 9. Micropore parameter curves of loess samples with different water contents.

5. Conclusions

The following conclusions can be drawn.

- (1) The uniform surface erosion stage of loess is dominated by water infiltration. In the stage of drop pit erosion, multiple drop pits will be formed on the slope surface due to differential erosion. In the beaded erosion stage of the drop pit, multiple drop pits are connected to each other. In the rill erosion stage, the drop pits have been connected to each other to form rills. The rills continue to develop and may form a slope rill network, slowing the erosion rate.
- (2) As the dry density increases, the various forces inside the loess body increase, resulting in increased impact resistance, reduced mud content, and reduced erosion. As the moisture content increases, the water collected in the pores increases, the contact points between the particles decrease rapidly, and the internal friction angle decreases sharply. The water-soluble cements and salts between the soil particles will gradually dissolve, and the cohesion of the soil will decrease. When the internal friction angle and cohesion of the two variables of shear strength decrease, the equivalent soil impact resistance also decreases, the mud content increases, and the amount of erosion increases.
- (3) With an increase of dry density, the total number of pores in remolded loess with different dry densities increases, the number of macropores decreases, and the average diameter of macropores decreases. The pore area of macropores and mesopores also decrease significantly, and the small pores and micropores increase.

- (4) In remolded loess, as the water content increases, the number of macropores increases significantly and the average pore diameter and pore area of macropores also increases significantly.

Author Contributions: Conceptualization, X.-A.L.; Formal analysis, Y.-H.D.; Funding acquisition, X.-A.L.; Methodology, Y.-H.D.; Supervision, X.-A.L.; Writing—original draft, H.Z.; Writing—review and editing, Z.-T.H. and F.W. All authors have read and agreed to the published version of the manuscript.

Funding: This research was funded by the Natural Science Foundation of China, grant numbers 42230712 and Shaanxi Coal Group Technology Project, grant numbers 2020SMHKJ-B-J-40.

Data Availability Statement: All data used in the study are confidential in nature, so the research data are not shared.

Acknowledgments: The work presented in this paper was supported by the National Natural Science Foundation of China (42230712) and Shaanxi Coal Group Technology Project (2020SMHKJ-B-J-40).

Conflicts of Interest: The authors declare that they have no known competing financial interests or personal relationships that could have appeared to influence the work reported in this paper.

References

- Liu, D.S. *Loess and Environment*; Science Press: Beijing, China, 1985; pp. 1–481.
- Derbyshire, E.; Mellors, T.W. Geological and geotechnical characteristics of some loess and loessic soils from China and Britain: A comparison. *Eng. Geol.* **1988**, *25*, 135–175. [[CrossRef](#)]
- Govers, G.; Poesen, J. Assessment of the interrill and rill contributions to total soil loss from an upland field plot. *Geomorphology* **1988**, *1*, 343–354. [[CrossRef](#)]
- Tang, Z.H.; Cai, Q.G.; Xu, F.; Zhu, Y.D. Study on soil erosion experiment monitoring and modeling of various scale conditions. *Adv. Water Sci.* **2002**, *13*, 781–787.
- Wirtz, S.; Seeger, M.; Ries, J.B. Field experiments for understanding and quantification of rill erosion processes. *Catena* **2012**, *91*, 21–34. [[CrossRef](#)]
- Pusch, R. Quick-clay microstructure. *Eng. Geol.* **1966**, *1*, 433–443. [[CrossRef](#)]
- Morgenstern, N.R.; Tchalenko, J.S. The Optical Determination of Preferred Orientation in Clays and Its Application to the Study of Microstructure in Consolidated Kaolin. II. *Proc. R. Soc. London Ser. A Math. Phys. Sci. R. Soc. Lond.* **1967**, *300*, 235–250.
- Smart, P. Soil structure in the electron microscope. In Proceedings of the International Conference of Structure, Solid Mechanics, and Engineering Design with Civil Engineering Materials, Southampton, UK, 11–13 September 1969.
- Brewer, R. Fabric and mineral analysis of soils. *Soil Sci.* **1965**, *100*, 73. [[CrossRef](#)]
- Smart, P. Optical Microscopy and Soil Structure. *Nature* **1966**, *210*, 1400. [[CrossRef](#)]
- Krizek, R.J.; Edil, T.B.; Ozaydin, I.K. Preparation and identification of clay samples with controlled fabric. *Eng. Geol.* **1975**, *9*, 13–38. [[CrossRef](#)]
- Gao, G.R. Classification of microstructure and collapsibility of loess. *Chin. Sci.* **1980**, *23*, 1203–1208.
- Lei, X.Y. Pore types and collapsibility of loess in China. *Chin. Sci.* **1987**, *17*, 1309–1318.
- Lei, X.Y. Characteristics of Huangshi pore near Xi'an. *Hydrogeol. Eng.-Ing Geol.* **1984**, *33*, 38–41.
- Lei, X.Y. Study on loess pore in Xi'an. *Quat. Res.* **1986**, *7*, 61–67.
- Bazant, Z.P.; Prat, P.C. Effect of Temperature and Humidity on Fracture Energy of Concrete. *Mater. J.* **1988**, *85*, 262–271.
- Bazant, Z.P.; Bishop, F.C.; Chang, T.P. Confined Compression Tests of Cement Paste and Concrete up to 300 ksi. *ACI J.* **1986**, *33*, 553–560.
- Li, Y.F. The porosity of Luochuan loess is studied by using the quantitative analysis results of micro-image microcomputer. *Site Investig. Sci. Technol.* **1990**, 6–9.
- Lin, R.S. Analysis of microstructure pore and water conductivity of Weibei loess. *Shaanxi Water Conserv.* **1990**, 43–47.
- Munkholm, L.J.; Heck, R.J.; Deen, B. Soil pore characteristics assessed from X-ray micro-CT derived images and correlations to soil friability. *Geoderma* **2012**, *181*, 22–29. [[CrossRef](#)]
- Ni, W.K.; Hua, S.Q. Influence of freezing-thawing cycles on micro-structure and shear strength of loess. *J. Glaciol. Geocryol.* **2014**, *36*, 922–927.
- Zhang, S.H.; Su, N.N.; Dong, X.Q. Microstructure Test of Loess under Different Consolidation Pressures. *Science Technol. Eng.* **2015**, *15*, 74–78.
- Li, C.H.; Fang, X.W.; Shen, C.N.; Ou, Y.X. Wetting-induced microstructural change of Q2 loess. *Sichuan Build. Sci.* **2016**, *3*, 40–45.

24. Zheng, H.; Li, X.A.; Deng, Y.H.; Li, J.; Wen, F. Physical Modelling of Hydraulic Erosion Rates on Loess Slopes. *Water* **2022**, *14*, 1344. [[CrossRef](#)]
25. Li, X.A.; Li, L.C. Quantification of the pore structures of Malan loess and the effects on loess permeability and environmental significance, Shaanxi Province, China: An experimental study. *Environ. Earth Sci.* **2017**, *76*, 523. [[CrossRef](#)]

Disclaimer/Publisher's Note: The statements, opinions and data contained in all publications are solely those of the individual author(s) and contributor(s) and not of MDPI and/or the editor(s). MDPI and/or the editor(s) disclaim responsibility for any injury to people or property resulting from any ideas, methods, instructions or products referred to in the content.